



Dacite formation at Ilopango Caldera, El Salvador: U-series disequilibrium and implications for petrogenetic processes and magma storage time

Jennifer M. Garrison

*Department of Geosciences and Environment, California State University, Los Angeles, California
90032, USA (jgarris@calstatela.edu)*

Mark K. Reagan

Department of Geoscience, University of Iowa, Iowa City, Iowa 52242, USA

Kenneth W. W. Sims

Departments of Geology and Geophysics, University of Wyoming, Laramie, Wyoming 82071, USA

[1] Ilopango Caldera was formed ~1810 years ago by eruption of the Tierra Blanca Joven (TBJ) dacite (70 km³) in central El Salvador. A subsequent eruption in 1880 produced a cluster of dacite domes in the center of Lago Ilopango that contain olive-bearing enclaves of basaltic andesite. The purpose of this study is to use trace element, isotope, and U-series data from the TBJ and 1880 eruptions to assess petrogenesis and the timescale of magma storage. We find that although the range of trace element data in the TBJ dacite can be reproduced by simple crystal fractionation of a plagioclase- and amphibole-rich mineral assemblage, the ⁸⁷Sr/⁸⁶Sr and ²⁰⁷Pb/²⁰⁴Pb data suggest that the 1880 basaltic andesite enclave has a different source than the dacites. This is consistent with U-series data that show the TBJ dacites have lower (²³⁰Th/²³²Th) than the 1880 basaltic andesite enclave (1.5 versus 1.6, respectively). All Ilopango rocks have ²³⁰Th excesses, and the range in (²³⁸U/²³²Th) of the TBJ dacites can be modeled by crystal fractionation of a mineral assemblage including accessory zircon and allanite from a magma that is similar in composition to the enclave. Mineral isochrons yield crystallization ages of <10,000 years, and disequilibrium (²²⁶Ra/²³⁰Th) values suggest a similarly short residence time. Our data suggest that the large volumes of erupted dacite at Ilopango Caldera are generated very rapidly.

Components: 9800 words, 13 figures, 3 tables.

Keywords: El Salvador; U-series; caldera; dacite; subduction; timescales.

Index Terms: 1031 Geochemistry: Subduction zone processes (3060, 3613, 8170, 8413); 1036 Geochemistry: Magma chamber processes (3618); 1120 Geochronology: Isotopic disequilibrium dating.

Received 20 February 2012; **Revised** 16 May 2012; **Accepted** 18 May 2012; **Published** 30 June 2012.

Garrison, J. M., M. K. Reagan, and K. W. W. Sims (2012), Dacite formation at Ilopango Caldera, El Salvador: U-series disequilibrium and implications for petrogenetic processes and magma storage time, *Geochem. Geophys. Geosyst.*, 13, Q06018, doi:10.1029/2012GC004107.

1. Introduction

[2] Ilopango Caldera is located in central El Salvador (N13.6780, W89.0444), 15 km east of the capital city of San Salvador (Figure 1). The lake filled caldera was formed during an explosive eruption 1810 years BP that produced the Tierra Blanca Joven (TBJ) dacite. Ilopango Caldera is one of many large calderas in Central America that have produced significant volumes of ash in the last 200 ka. Deposits from similar calderas such as Aitlán, Ayarza, Coatepeque, Apoyo, Los Chocoyos and Apoyeque have been found in Quaternary deposits throughout Central America, the eastern Pacific Ocean basin [Kutterolf *et al.*, 2008a, 2008b; Sussman, 1985; Vogel *et al.*, 2006; Rose *et al.*, 1999; Mehringer *et al.*, 2005] and the Caribbean seafloor [Jordan *et al.*, 2006; Sigurdsson *et al.*, 2000; Carey and Sigurdsson, 2000]. The sources and volumes of these ignimbrites and tephra layers have been documented in the foundational studies of Bice [1985], Sussman [1985], Rose *et al.* [1979], Carr *et al.* [2003, 1990], and Carr [1984]. Recent research has provided further insight into silicic magma production rates and volumes [Kutterolf *et al.*, 2007, 2008a, 2008b; Mehringer *et al.*, 2005], as well as the petrogenesis of large volumes of dacite and rhyolite [Vogel *et al.*, 2006; Bachmann and Bergantz, 2004], however the storage times of magma in these large caldera storage systems is largely unknown.

[3] In this paper we present new geochemical data from the Ilopango TBJ dacites and the post-caldera lavas and mafic enclaves, including U-series data on whole rocks and mineral and glass separates. The Ilopango eruptive products are ideal for ^{238}U - ^{230}Th and ^{226}Ra - ^{230}Th disequilibria studies as they are <1800 years old and allow for robust interpretation of the measured disequilibria, they range from basaltic andesite to rhyolite and the deposits are moderately crystal-rich. We show that, despite a large volume of erupted dacite, the minerals do not record a protracted storage time, but instead record generation of the silicic magmas only a short time (<10,000 years) before eruption, which was most likely triggered by an influx of mafic magma that represents a different magmatic lineage.

2. Geologic Background

[4] The Central American Volcanic Arc (CAVA) results from subduction of the Cocos Plate beneath the Caribbean Plate [DeMets, 2001]. The dip of the slab beneath El Salvador is 55° , and it gradually

increases to 75° beneath Nicaragua before progressively flattening as the trench approaches the subducting Cocos Ridge in Panama [Carr *et al.*, 1990; MacKenzie *et al.*, 2010]. The convergence rate in El Salvador is 70 mm yr^{-1} [DeMets, 2001; DeMets *et al.*, 1990], and the crust is estimated to be 32–38 km thick [Carr, 1984]. The caldera-forming eruption of Ilopango produced 70.6 km^3 of dacite (18 km^3 onshore, 52.6 km^3 offshore [Kutterolf *et al.*, 2008b]) and resulted in formation of the $8 \times 11 \text{ km}$ caldera that is now the location of Lago Ilopango [Rose *et al.*, 1999]. The TBJ ignimbrites from this cataclysmic eruption blanket much of El Salvador and have been traced as far away as the Greenland ice sheet [Zielinski, 2000]. An initial ^{14}C eruption age for TBJ of 1605 ± 20 years BP was established by Dull *et al.* [2001], however a revised ^{14}C age of 1810 ± 30 years BP was determined by Mehringer *et al.* [2005]. The TBJ eruption is considered to be a major archeological event that altered local cultures [Dull *et al.*, 2001] and is frequently used as a time-stratigraphic marker [Mehringer *et al.*, 2005]. Outcrops of the TBJ ignimbrites near Lago Ilopango are up to 30 m thick and contain white pumice clasts that are up to 10 cm in diameter. Individual pulses of this ignimbrite are subdivided into six units referred to as TBJ-A (oldest) – TBJ-F (youngest). Where observed, the contact between these units is a well-defined but uneven erosional boundary. The A unit is recognized as a crossbedded basal surge deposit (<1 m thick) that contains a small percent of pumice and abundant lithics. The B - F units represent the main phase of explosive activity [Mehringer *et al.*, 2005]. Older eruptions are referred to as TB-2 through TB-4 [Rose *et al.*, 1999]; the 36.3 km^3 TB-4 ash has been dated at 36 ka and the TB-2 has been dated at 15 ka [Lexa *et al.*, 2011; Kutterolf *et al.*, 2008b]. An eruption of a lava dome in 1880 produced a cluster of rocky islands located in the center of Lago Ilopango, called Cerros Quemadas. The dacite from this rocky outcrop contains olivine-bearing mafic enclaves of basaltic andesite. Another island in Lago Ilopango, Il Pat, is composed entirely of flow banded rhyolite and its eruption age is only constrained to post-date the TBJ eruption.

3. Petrography

[5] In general, all pumice clasts from the TBJ units are highly vesicular, moderately crystal-rich (10–15%) and contain plagioclase and hornblende as the primary mineral assemblage. Trace amounts of clinopyroxene, apatite and oxides are observed in

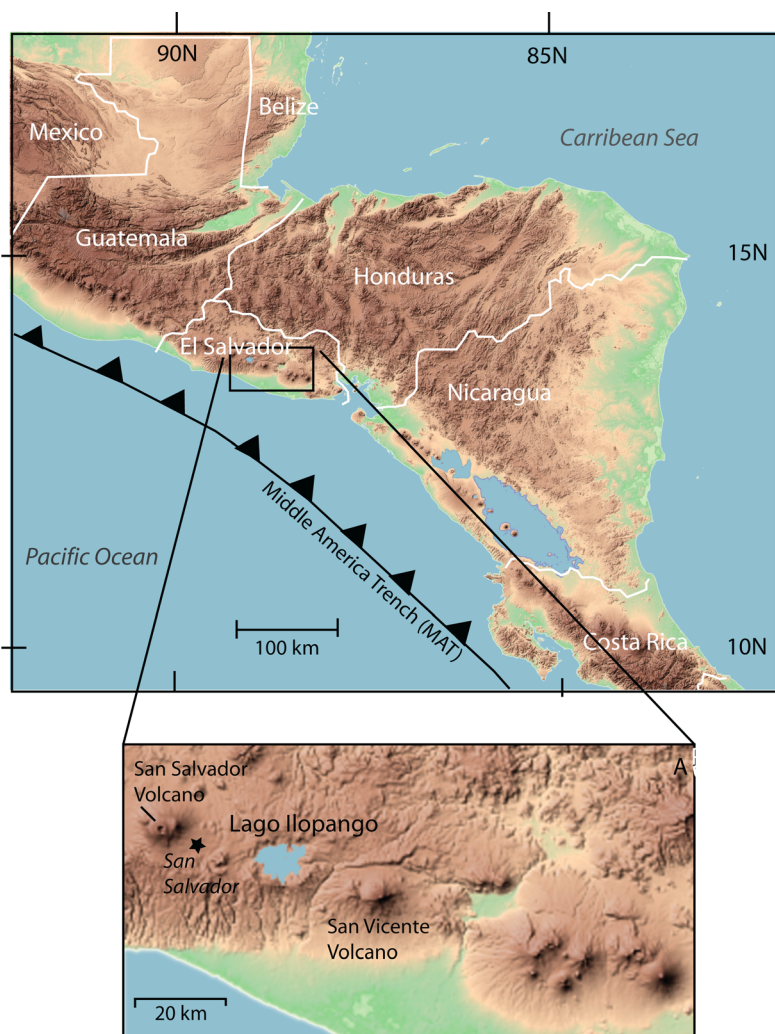


Figure 1. Location map of Central America, showing the location of Ilopango Caldera (Lago Ilopango), the capital city of San Salvador, as well as two nearby volcanoes, San Salvador and San Vicente.

the matrix and as inclusions in the crystals. The mineralogy of the TBJ-B unit consists predominantly of plagioclase (80%) and hornblende (20%), with trace amounts of clinopyroxene and oxides. The plagioclase crystals are 2–3 mm in length, euhedral to subhedral and comprise two populations, those that have sieve texture cores (Figure 2a) and those that are pristine. The sieve texture cores have abundant inclusions of glass and minerals, including apatite, oxides and clinopyroxene and comprise 2–3% of the crystals. The pristine plagioclase crystals contain 1% apatite inclusions that are generally parallel to the growth zones (Figure 2b). The hornblende crystals (1 mm in length) are euhedral to subhedral and also comprise two populations; those that have pristine rims with abundant apatite, orthopyroxene inclusions (Figures 2c and 2d) and oscillatory zoning, and those that have

reaction rims and are nearly completely dissolved. Both the plagioclase and the hornblende crystals in TBJ-B occur as individual crystals, not intergrowths. The mineralogy of the TBJ-E unit is very similar to the TBJ-B unit in terms of texture and crystal populations, except that there are intergrowths of plagioclase and hornblende, and the percentage of hornblende is slightly higher. The mineralogy and texture of the TBJ-F unit is identical to the TBJ E unit, and includes abundant intergrowths of plagioclase and hornblende. Overall, the TBJ dacite assemblage comprises plagioclase (75%), hornblende (20%), orthopyroxene (3%) and 2% accessory clinopyroxene + magnetite + ilmenite + apatite.

[6] Unlike the TBJ dacites, the 1880 Cerros Quemadas dacite dome is crystal rich (40% crystals,

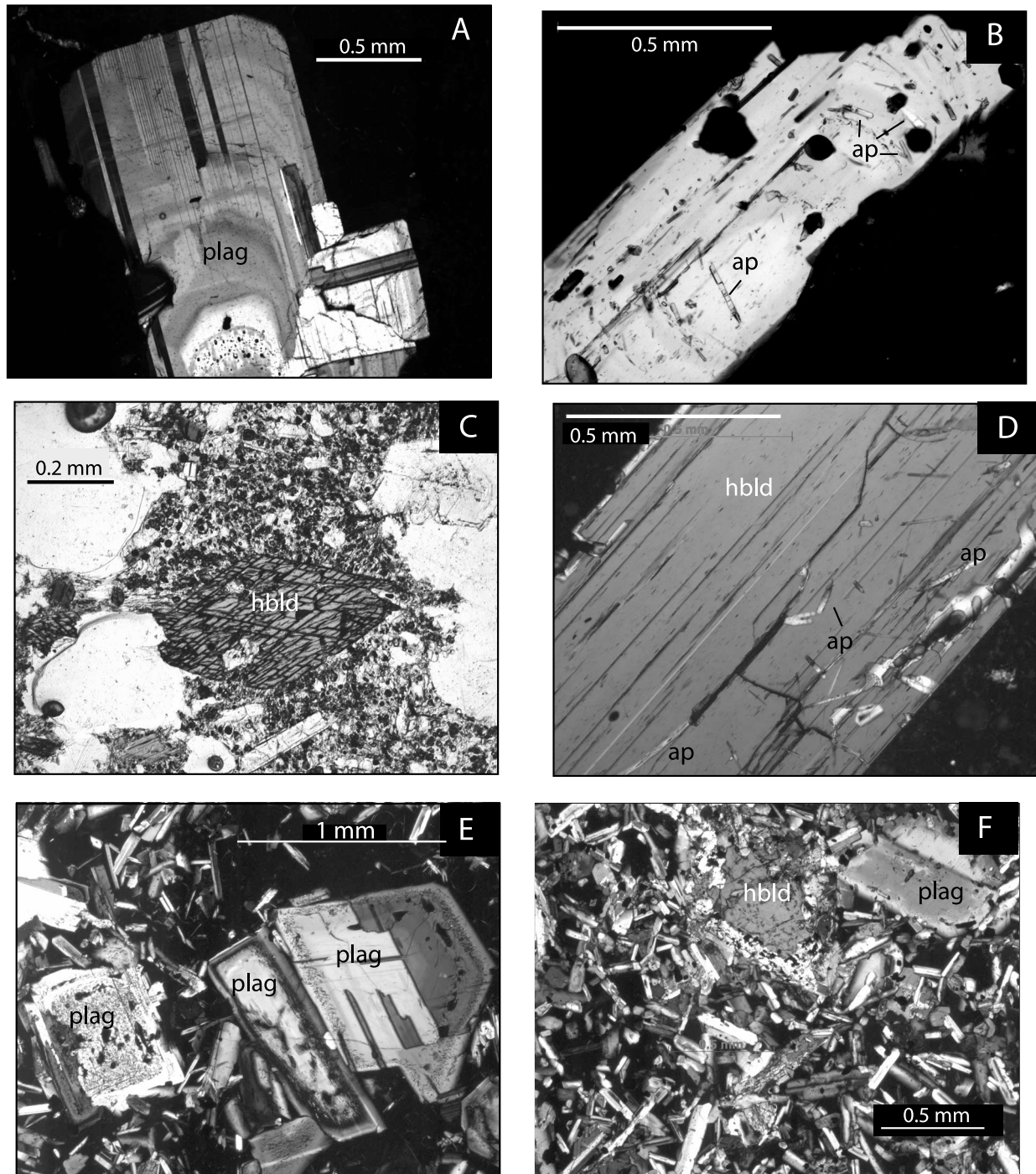


Figure 2. Photomicrographs of Ilopango rocks, showing (a) euhedral plagioclase crystal with sieve-texture core in the TBJ “F” pumice, (b) euhedral plagioclase containing melt inclusions and apatite inclusions parallel to growth rims, (c) pristine hornblende in the TBJ “C” pumice, (d) euhedral hornblende crystal containing apatite crystals, (e) multiple populations of plagioclase crystals in the Islas Quemadas mafic enclave, and (f) resorbed hornblende and plagioclase in the dacite dome lava.

60% matrix) and contains phenocrysts of plagioclase (2 mm) and olivine (1 mm) in a fine grained matrix of lath-shaped plagioclase (0.2–0.4 mm), hornblende and clinopyroxene. The plagioclase

phenocrysts include three populations, those that are euhedral, those that have euhedral rims with resorbed, glass-inclusion-rich cores (Figure 2e), and those that have euhedral cores with resorbed

rims. This dacite also has compact clots of fine-grained (0.1–0.5 mm) hornblende and plagioclase intergrowths. The mafic enclave is petrographically similar to the dacite dome, although it contains a higher percentage of hornblende in the matrix along with a trace amount of orthopyroxene. In many cases the hornblende has been partially dissolved (Figure 2f).

4. Analytical Methods

[7] Six samples were analyzed from Ilopango caldera, including units B, C and F of the TBJ tephra, the mafic enclave the host dacite from Cerros Quemadas, and the flow-banded rhyolite from Il Pat dome. Samples were washed in ultrapure water before methodical removal of weathered rims. A fraction of crushed rock was powdered in a Spex Al-ceramic shatterbox and sent to Michigan State University (MSU) for ICP and XRF analyses; the remainder was used for mineral separations. Sample powders were analyzed at MSU for trace elements using the Platform Inductively Coupled Plasma-Mass Spectrometer (ICP-MS) following procedures outlined by *Johnson et al.* [1999], and for major elements using the Bruker S4 PIONEER 4 kW wavelength dispersive X-ray fluorescence spectrometer following procedures outlined by *Johnson et al.* [1999], *Knaak et al.* [1994], and *Deering et al.* [2008]. Rocks were dissolved in ultra-pure HF-HNO₃-HCl acid using high pressure vessels, and then separated by aliquots for Sr, Nd, Pb, U, Th and Ra analyses. In order to determine if zircon had dissolved during bombing, several samples were also digested in 15 ml Teflon beakers. Chemical separation of Sr, Nd and Pb were conducted in the University of Iowa clean lab using Eichrom Sr-spec (Sr and Pb) and Ln-spec (Nd) resins. Separation of U-Th and Ra isotopes was conducted in the clean lab at Woods Hole Oceanographic Institute (WHOI) using established protocols [*Sims et al.*, 2008a, 2008b]. Glass and mineral separates (amphibole, pyroxene, plagioclase and magnetite) from Ilopango units B, E and F were separated at the University of Iowa using a combination of magnetic separation and hand-picking. Silicate mineral separates were hand-picked to 99% purity, leached in a 10% HF solution before being crushed to a fine powder. All mineral separates were dissolved using HF-HNO₃-HCl acids followed by fuming with boric and perchloric acids. Aliquots of whole rock, glass and mineral solutions for isotope dilution (ID) measurements were spiked with ²²⁹Th and ²³³U, allowed to

equilibrate for 48 hours then put through anion resin columns in order to separate Ra from U and Th. The Ra aliquot was spiked with ²²⁸Ra and put through several cation resin columns. Immediately before analysis, anion resin was used as the final clean-up column following the procedures established by *Sims et al.* [2008b] in order to separate ingrown ²²⁸Th. Ra, Th, U, Nd, Sr, and Pb isotopes were measured at WHOI using the Thermo-Finnigan NEPTUNE Plasma ionization multicollector mass spectrometer following procedures outlined by *Sims et al.* [2008a]. For Sr and Nd the internal precision is 5–10 ppm (2σ); external precision after adjusting to 0.71024 (NBS SRM 987) and 0.511847 (La Jolla Nd standard), respectively, is estimated to be 15–30 ppm. Pb analyses have internal precisions of 15–30 ppm; SRM 997 Tl was used as an internal standard, and then normalized to NBS 981 using the values of *Todt and Cliff* [1996]. External reproducibility (including full chemistry) for ²⁰⁸Pb/²⁰⁴Pb, ²⁰⁷Pb/²⁰⁴Pb, and ²⁰⁶Pb/²⁰⁴Pb are 150–200 ppm (2σ) and 90 ppm (2σ) for ²⁰⁸Pb/²⁰⁶Pb. ²³⁴U/²³⁸U was measured following the procedures established by *Ball et al.* [2008] and *Sims et al.* [2008a, 2008b]. ²³⁰Th/²³²Th was also measured using WHOI's ThermoFisher NEPTUNE and procedures by *Ball et al.* [2008] and *Sims et al.* [2008b, 2008c]. Reproducibility is within propagated analytical errors, which takes into account uncertainties in spike calibrations and tail corrections and decay constants (less than 2σ). ²³⁸U and ²³²Th concentrations were measured by isotope dilution on a single collector sector ICPMS (ThermoFisher Element) at WHOI. ²²⁶Ra concentrations were measured by isotope dilution mass spectrometry using WHOI's ThermoFisher NEPTUNE using techniques developed *Sims et al.* [2008b, 2008c]. Minerals from the dacite units E, F and B were separated by hand-picking, mounted in epoxy and analyzed for major and minor elements using the Cameca JXA-8200 Super-probe at UCLA. Mineral data are given in Table S1 in the auxiliary material.¹

5. Results

[8] Major and trace element data are presented in Table 1. All samples fall into the medium K₂O sub-alkaline group based on the classification system of *Le Maitre et al.* [1989] (Figure 3a), and are similar to the overall composition of volcanic rocks from El Salvador (shaded field in Figure 3a). Variations in major element compositions for the Ilopango samples are considered typical of subduction zone

¹Auxiliary materials are available in the HTML. doi:10.1029/2012GC004107.

Table 1. Major and Trace Element Data From Rocks of Ilopango Caldera

	Unit B	Unit E	Unit F	Ilo 5	Ilo 6	Ilo 7
SiO ₂ (wt %)	69.73	69.83	69.71	68.26	56.21	72.72
TiO ₂ (wt %)	0.33	0.33	0.32	0.42	0.74	0.28
Al ₂ O ₃ (wt %)	14.82	14.67	14.81	15.67	17.7	14.07
Fe ₂ O ₃ (wt %)	2.8	2.88	2.85	4.01	8.24	2.2
MnO (wt %)	0.11	0.11	0.1	0.12	0.16	0.09
MgO (wt %)	0.84	0.83	0.86	1.41	3.72	0.53
CaO (wt %)	2.97	2.88	3.02	3.91	7.44	2.11
Na ₂ O (wt %)	4.12	4.15	4.06	4.16	3.17	4.38
K ₂ O (wt %)	2.14	2.16	2.15	1.93	1.1	2.34
P ₂ O ₅ (wt %)	0.1	0.1	0.11	0.14	0.15	0.15
Total (wt %)	97.96	97.94	97.99	100.03	98.63	98.87
U (ppm)	1.46	0.98	1.37	1.27	0.60	1.26
Rb (ppm)	44	45	43	39	19	49
Zr (ppm)	163	165	162	151	98	181
Sr (ppm)	286	281	291	330	467	254
Th (ppm)	3.77	2.07	2.89	2.78	1.20	2.71
Nb (ppm)	2.85	3.21	3.09	2.54	1.99	3.23
Ba (ppm)	1061	1086	1064	978	535	1192
La (ppm)	12.11	12.4	11.98	11.46	8.67	13.15
Ce (ppm)	27.24	28.18	27.29	26.43	18.56	28.74
Pr (ppm)	3.38	3.44	3.37	3.24	2.8	3.49
Nd (ppm)	12.65	12.92	12.73	12.34	12.49	13.29
Sm (ppm)	2.72	2.84	2.7	2.62	3.14	2.76
Eu (ppm)	0.81	0.84	0.84	0.86	0.99	0.81
Gd (ppm)	2.61	2.69	2.56	2.72	3.24	2.78
Tb (ppm)	0.44	0.44	0.43	0.43	0.52	0.44
Dy (ppm)	2.52	2.43	2.5	2.57	3.23	2.55
Y (ppm)						
Ho (ppm)	0.51	0.5	0.49	0.52	0.67	0.53
Er (ppm)	1.63	1.62	1.58	1.6	2	1.7
Yb (ppm)	1.96	1.96	1.87	1.94	2.01	2.04
Lu (ppm)	0.32	0.32	0.33	0.31	0.32	0.34
Hf (ppm)	3.8	3.9	3.7	3.6	2.8	4.4
Ta (ppm)	0.62	0.67	0.6	0.53	0.18	0.84
Pb (ppm)	10.1	11.4	10.8	9.5	6.5	10.4

^aTrace elements were measured using the Platform (ICP-MS) at MSU following procedures outlined in *Deering et al.* [2008]. Major elements were analyzed using a Bruker S4 PIONEER-wavelength dispersive XRF.

volcanic rocks, including decreasing CaO, Al₂O₃, FeO and MgO with increasing SiO₂ (Figure 3b) that often is attributed to plagioclase + pyroxene + magnetite +/- olivine +/- amphibole fractionation during differentiation [e.g., *Gill*, 1981]. The 1880 Cerros Quemadas dacite is similar in major element composition to the TBJ dacites. The mafic enclaves within the dacite are basaltic andesites. The only true rhyolite in this study is the sample from the Il Pat dome.

[9] Primitive-mantle normalized trace element data are shown on incompatible trace element (ITE) and rare earth element (REE) diagrams (Figure 4). Samples show typical subduction zone characteristics, including relative depletions in Ta, Nb and

Ti, and elevated concentrations of large ion lithophile elements (LILE) with respect to rare earth elements (REE). Primitive-mantle normalized REE patterns are U-shaped with strong enrichments in light REE and weak enrichments in heavy REE over middle REE for the dacites. The REE pattern of the mafic enclave is similar to that of the dacites, but has lower concentrations of light REE, and higher concentrations of middle REE.

[10] Long-lived isotope data are listed in Table 3 and shown in Figure 5. Our data are consistent with previously reported values for El Salvador, showing a positive correlation between ⁸⁷Sr/⁸⁶Sr and ¹⁴³Nd/¹⁴⁴Nd that is a feature of CAVA rocks (Figure 5a). This unusual positive correlation in CAVA rocks has been explained by variable degrees of melting of mantle associated with a flux of fluid derived from marine sediment (model shown in Figure 5a) [*Feigenson and Carr*, 1986; *Carr et al.*, 1990]. Ilopango samples have ²⁰⁶Pb/²⁰⁴Pb and ²⁰⁷Pb/²⁰⁴Pb values that range from 18.619–18.942 and 15.557–15.624, and plot within previously established data fields for Central American rocks (Figure 5b). The mafic enclave from Ilopango has the highest ²⁰⁶Pb/²⁰⁴Pb and ²⁰⁷Pb/²⁰⁴Pb values that trend toward the metamorphic basement value of *Feigenson and Carr* [1993].

[11] U-series whole rock analyses are given in Table 2 and shown in Figure 6a. All samples in this study are characterized by (²³⁰Th/²³⁸U) > 1.0, with ²³⁰Th excesses ranging from 1.6% (unit F) to 9.0% (dacite dome). The basaltic andesite enclave has (²³⁰Th/²³⁸U) = 1.04. None of the observed excesses correlate with SiO₂ or MgO concentrations. The (²³⁰Th/²³²Th) values range from 1.5 for the TBJ dacites to 1.6 in the mafic enclave. Mineral-separate data from the three Ilopango TBJ units (B, E and F) are shown in Figure 6b. The data form linear arrays that overlap the range of whole rock values, except for the F-unit amphibole that has (²³⁸U/²³²Th) of 2.8 and an age corrected (²³⁰Th/²³²Th) 1.49, lower than the whole rock and mineral average of 1.51. Age corrected data and the modified York regression method [*Mahon*, 1996] were used to calculate the isochron ages for the mineral arrays. The averaged isochron age for units E, F and B is <4000 years, however given the scatter of the data, the linear array can only be reasonably constrained to an age range consistent with crystal growth of less than 10,000 years.

[12] Age-corrected ²²⁶Ra values for Ilopango whole rocks and glasses are shown in Table 3 and Figure 7. The mafic enclave has the highest age-corrected

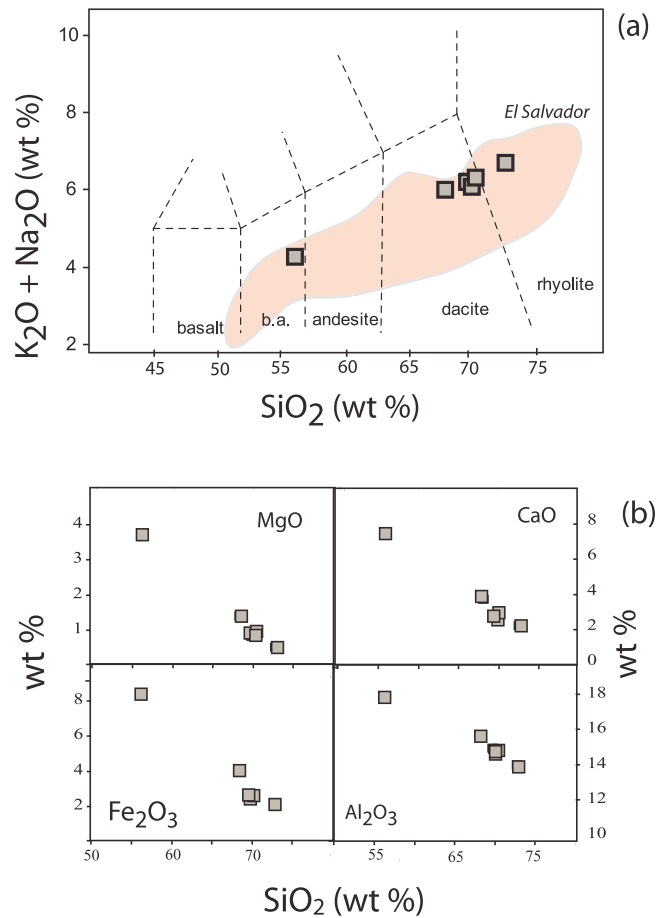


Figure 3. (a) TAS diagram showing the range in major element compositions normalized to 100% of the Ilopango rocks (classification from *Le Maitre et al.* [1989]) and the range of values for volcanic rocks from El Salvador. Shaded region from *Vogel et al.* [2006]. (b) Wt % SiO₂ versus weight % MgO, CaO, Al₂O₃ and Fe₂O₃ for the Ilopango rocks.

(²²⁶Ra/²³⁰Th) of 1.12, and the dacite whole rocks and glasses have (²²⁶Ra/²³⁰Th) ranging from 1.02 to 0.82 (Figure 7a). The most evolved (i.e., highest SiO₂) samples have the greatest ²²⁶Ra depletion with respect to ²³⁰Th (Figure 7b).

[13] Electron microprobe data from the Ilopango minerals show that the plagioclase crystals from all three units range from An₄₉-An₇₇ (Figure S1) and have less than 0.3 weight % K₂O (Table S1). There is no consistent trend between core and rim compositions, and crystals from all three units vary among normal, reverse and oscillatory zonation. All analyzed pyroxene are orthopyroxene (Di₂En₅₀₋₅₈) (Figure S1); orthopyroxene and hornblende have abundant inclusions of apatite and Fe-Ti oxides (Figure S2). The composition of the matrix glass ranges from 79 to 81 wt % SiO₂, consistent with the composition of glass inclusions in the plagioclase and hornblende, which are range from 79 to 80 wt %

SiO₂. Glass inclusions in the orthopyroxene and hornblende range from 56 to 58 wt % SiO₂.

6. Discussion

6.1. Magma Differentiation at Ilopango Caldera

[14] The trace element variation observed in the Ilopango rocks is typical of arc rocks. In general, the Ta-Nb depletion in arc lavas is presumed to be a characteristic of the source and reflects the sequestering of Ta and Nb in a residual mantle phase [*Tiepolo et al.*, 2001; *Reagan and Gill*, 1989], or alternatively the relatively low mobility of Ta and Nb in fluids from the subducting slab [*Schmidt et al.*, 2004]. The enrichment in the LILE and LREE concentrations is attributed to the slab fluid component as well as to the relative incompatibility of these elements during crystallization

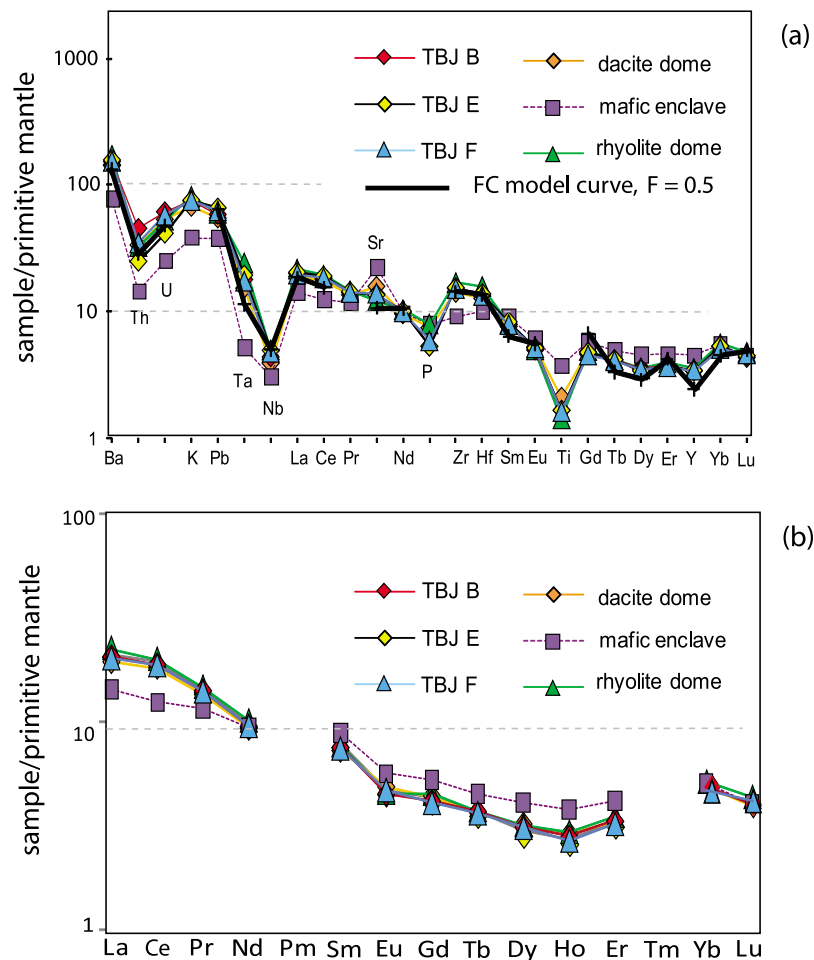


Figure 4. (a) Primitive mantle-normalized incompatible trace element (ITE) diagram for rocks from Ilopango Caldera. The heavy black line superimposed on the data is a model curve representing 50% crystallization of basaltic andesite. Bulk distribution coefficients were calculated using partition coefficients from published literature and equations for equilibrium crystallization. (b) Rare earth element (REE) diagram for the Ilopango samples. Normalization factors from *Sun and McDonough* [1989].

[*Hawkesworth et al., 1997; Davidson, 1996*]. The TBJ samples have greater relative depletions in the MREE than the 1880 samples; a trait that is commonly attributed to amphibole fractionation [*Davidson et al., 2007*]. The geochemical similarities in the Ilopango rocks suggest a common lineage, in which the trace element variation can be modeled without assimilation, using an assemblage of plagioclase (70%) + amphibole (20%) + orthopyroxene (5%) + olivine (5%) + magnetite (0.01%) + zircon (0.004%) + apatite (0.001%) +/– allanite (0.001%) at 50% crystallization (Figure 4a). However, either the basaltic andesite does not represent a parental magma for the TBJ dacites, or crustal assimilation contributes to differentiation (AFC). This is indicated by the differences in $^{87}\text{Sr}/^{86}\text{Sr}$, $^{143}\text{Nd}/^{144}\text{Nd}$ and $^{207}\text{Pb}/^{204}\text{Pb}$ values between the

basaltic andesites and dacites (Figure 5), as well as the positive correlation between the isotope values and weight % SiO_2 (Figure 8).

[15] The TBJ dacites and the dacite dome have higher $^{143}\text{Nd}/^{144}\text{Nd}$ than the basaltic andesite (Figure 5a), and in the CAVA, high-Nd isotope values are typically attributed to a depleted mantle source [*Carr et al., 1990*] or to assimilation of the ultramafic high-Nd forearc crust of the Chortis Block [*Geldmacher et al., 2008*]. Figure 5a shows a mixing curve between a 5% melt of Chortis forearc sediment and the Ilopango basalt andesite. This curve shows that 20–30% of the sediment melt is required to account for increase in $^{87}\text{Sr}/^{86}\text{Sr}$ and $^{143}\text{Nd}/^{144}\text{Nd}$ in the dacites. The Carr model requires much lower percent of high-Nd slab fluid. Either of these models can account for the variations in Sr and

Table 2. U-Series Data for Ilopango Whole Rocks, Mineral Separates and Glass

	U (ppm)	$(^{238}\text{U}/^{230}\text{Th})$	Th (ppm)	$(^{238}\text{U}/^{232}\text{Th})$	Error	$(^{230}\text{Th}/^{232}\text{Th})$	Error	$(^{230}\text{Th}/^{232}\text{Th})$ Age Corr.	$(^{226}\text{Ra}/^{230}\text{Th})$	Error	$(^{226}\text{Ra}/^{230}\text{Th})$ Age Corr.
<i>Whole Rock Data</i>											
Ilopongo B	1.46	0.98	3.77	1.482	0.003	1.515	0.003	1.516	0.968	0.004	0.936
Ilopongo E	0.98	0.95	2.07	1.447	0.003	1.523	0.003	1.524	1.026	0.004	1.051
Ilopongo F	1.37	0.98	2.89	1.492	0.003	1.516	0.003	1.517			
Ilopongo 5a	1.27	0.91	2.78	1.387	0.003	1.526	0.003	1.526	1.005	0.003	1.009
Ilopongo 6	0.60	0.96	1.20	1.516	0.003	1.579	0.003	1.580	1.117	0.004	1.232
Ilopongo 7	1.26	0.93	2.71	1.408	0.003	1.508	0.003	1.508	0.929	0.004	0.859
TML (n = 5)	10.64	1.02	30.58	1.059	0.002	1.082	0.001	na	1.010	0.002	na
AThO (n = 3)	2.32	1.09	7.61	0.928	0.002	1.020	0.001	na	1.030	0.002	na
<i>Mineral Separates and Glass</i>											
Unit B											
Glass	1.57	0.892	3.56	1.345	0.003	1.507	0.003	1.509	0.909	0.003	0.820
Magnetite	0.28	1.013	0.55	1.537	0.003	1.518	0.003	1.518			
Pyroxene	0.14	0.987	0.28	1.504	0.003	1.525	0.003	1.525			
Unit E											
Glass	1.83	0.938	3.96	1.411	0.003	1.504	0.003	1.506	0.974	0.003	0.948
Amphibole	0.09	0.808	0.22	1.217	0.003	1.506	0.002	1.510			
Magnetite	0.29	1.043	0.57	1.574	0.003	1.509	0.003	1.508			
Pyroxene	0.15	0.990	0.31	1.496	0.003	1.511	0.003	1.512			
Unit F											
Glass	1.31	0.981	2.67	1.492	0.003	1.521	0.003	1.521			
Amphibole	0.13	1.874	0.15	2.823	0.003	1.506	0.006	1.490			
Magnetite	0.23	1.047	0.43	1.593	0.003	1.522	0.003	1.521			
Plagioclase	0.13	0.949	0.29	1.433	0.003	1.511	0.003	1.512			
Pyroxene	0.12	0.985	0.25	1.498	0.003	1.521	0.003	1.522			

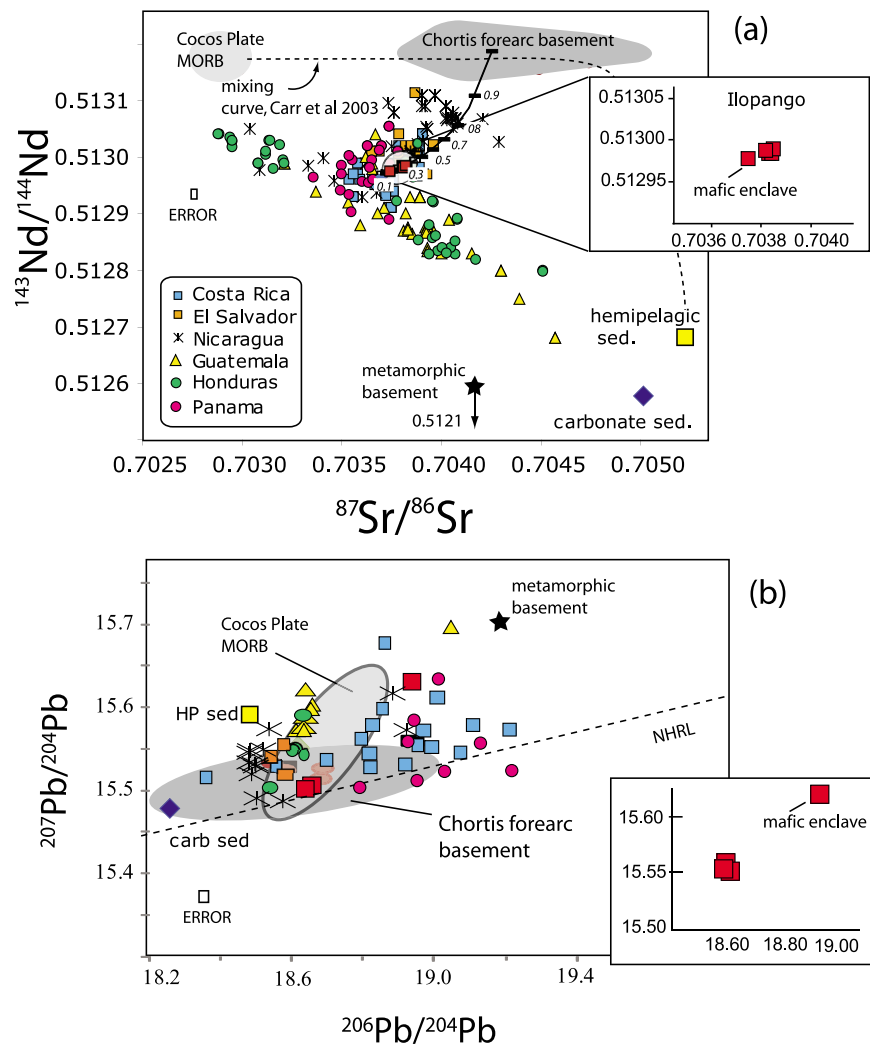


Figure 5. (a) $^{87}\text{Sr}/^{86}\text{Sr}$ versus $^{143}\text{Nd}/^{144}\text{Nd}$ data for the Ilopango and CAVA rocks; data for CAVA samples from *Feigenson and Carr* [1986]. Inset expanded field shows the Ilopango data. The solid black line represents a modeled mixing curve between the mantle array and 5% melt of the forearc basement of the Chortis Block; small italicized numbers represent the proportion of Chortis block crust in the mixture. The dashed line represents the sediment-mantle mixing model of *Feigenson and Carr* [1986]. Data from *Geldmacher et al.* [2008]. Fields for Cocos Plate MORB, sediment and metamorphic basement from *Feigenson and Carr* [1986]. (b) $^{207}\text{Pb}/^{204}\text{Pb}$ isotope data for the Ilopango rocks. NHRL = Northern Hemisphere Reference Line from *Zindler and Hart* [1986]. Symbols are the same as in Figure 5a.

Nd isotope values. However, the $^{207}\text{Pb}/^{204}\text{Pb}$ and $^{206}\text{Pb}/^{204}\text{Pb}$ of the basaltic andesite is consistent with neither sediment fluid nor Chortis block sediment melt, but trends toward metamorphic basement (Figure 5b). This inconsistency points toward our initial hypothesis that the basaltic andesite is not a parental magma for the TBJ dacites, but likely triggered the 1880 lava dome activity by injection into the base of caldera.

[16] The 50–60% fractional crystallization that is sufficient to generate the observed variation without significant crustal assimilation (Figure 4a) is

also consistent with the proportions of minerals observed in thin section as well as the trace element ratios, including Sr concentrations, U/Th, La/Dy and La/Yb (Figure 9). The Sr and La/Dy values (controlled by plagioclase and hornblende, respectively) can be reproduced using a composition similar to the basaltic andesite using the same mineral proportions. The minerals that provide the most leverage over the whole-rock $(^{238}\text{U})/(^{230}\text{Th})$ concentrations are accessory phases like allanite, apatite, monazite and zircon. Due to the high crystal/magma partition coefficients, even small amounts of these minerals provide ample leverage on the U/Th

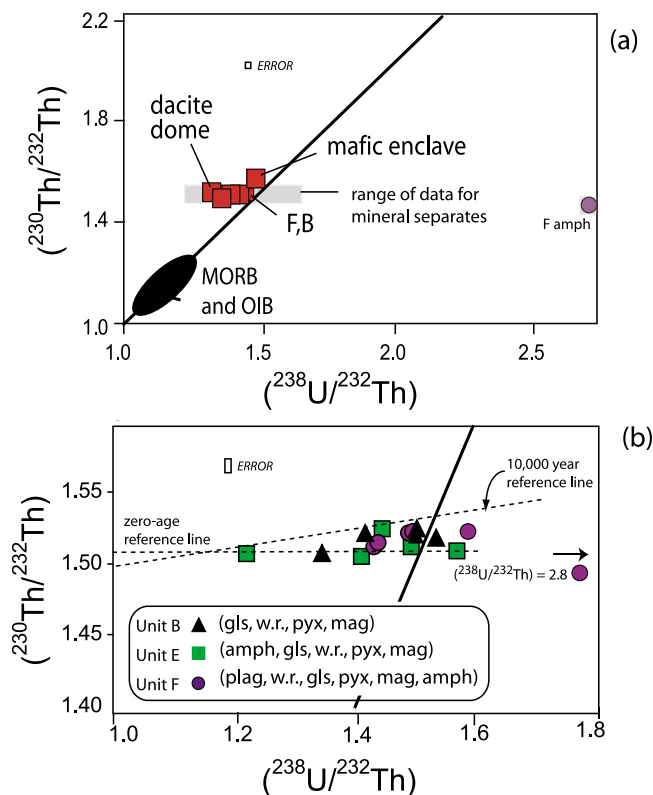


Figure 6. (a) Equiline diagram showing whole-rock U-series data from Ilopango Caldera. Field for error bars is shown on graph. Field for MORB and OIB is from *Walker et al.* [2007]. Purple circle symbol represents the amphibole mineral separate value from B. (b) Age-corrected mineral separate data for the Ilopango samples. The minerals are listed in the order that they appear on the graph. The horizontal dashed line is the zero-age reference line, the 10,000 year reference line is shown for comparison.

of igneous rocks [*Schmitt, 2011*] without significantly changing the major element composition of the magma. For example, U/Th in the Ilopango samples is poorly correlated with weight % MgO and P₂O₅ and Zr concentrations (Figure 10). However, the U/Th values cannot be explained without crystallization of accessory zircon and allanite (Figure 9b). If the 1880 dacite is excluded from Figures 10a–10c, there are indeed consistent trends between U/Th on the MgO and Zr ppm. The weak colinearity on Figure 10 might reflect the slightly different composition of the 1880 dacite compared to the TBJ tephtras, suggesting that neither of the

1880s lavas is directly linked to the TBJ tephtras. Nonetheless, the overall similarity in compositions suggests that they were generated from similar sources and followed similar liquid lines of descent.

6.2. U-Series Evidence for Magma Genesis at Ilopango

[17] Several studies have reported U-series data for CAVA rocks [*Reagan and Gill, 1989; Reagan et al., 1994; Herrstrom and Reagan, 1995; Clark et al., 1998; Thomas et al., 2002; Tepley and Lundstrom, 2006; Walker et al., 2007; Jicha and*

Table 3. Isotope Data for Ilopango Caldera, El Salvador

	⁸⁷ Sr/ ⁸⁶ Sr	Error (10 ⁻⁶)	Sr (ppm)	¹⁴³ Nd/ ¹⁴⁴ Nd	Error (10 ⁻⁶)	Nd (ppm)	²⁰⁶ Pb/ ²⁰⁴ Pb	²⁰⁷ Pb/ ²⁰⁴ Pb	²⁰⁸ Pb/ ²⁰⁴ Pb	Error (10 ⁻³)	Pb (ppm)
Ilopango B	0.703815	6	286	0.512982	4	12.65	18.617	15.557	38.289	0.8	10.12
Ilopango E	0.703820	7	281	0.512986	6	12.92	18.615	15.556	38.288	0.8	11.36
Ilopango F	0.703804	7	291	0.512985	7	12.73	18.618	15.558	38.295	0.8	10.82
Ilopango 5a	0.703745	7	330	0.512976	7	12.34	18.942	15.624	38.493	0.8	9.47
Ilopango 6	0.703810	7	467	0.512982	7	12.49	18.619	15.557	38.291	0.8	6.54

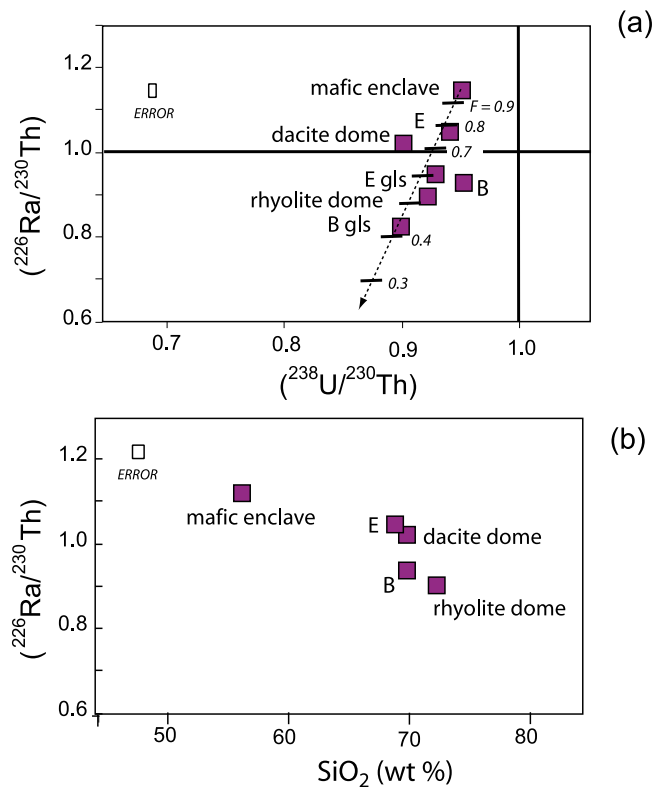


Figure 7. (a) Age-corrected ^{226}Ra data versus $(^{238}\text{U}/^{230}\text{Th})$ for the Ilopango whole rocks, mineral separates and glasses. The dark line represents secular equilibrium between ^{226}Ra and ^{230}Th . The dashed arrow shows a fractional crystallization model and was calculated using the same D values for Figure 4a. D_{Ra} and D_{Th} are from *Fabrizio et al.* [2010]. Italicized numbers represent the fraction of melt remaining. (b) ^{226}Ra data versus weight % SiO_2 for the Ilopango whole rocks.

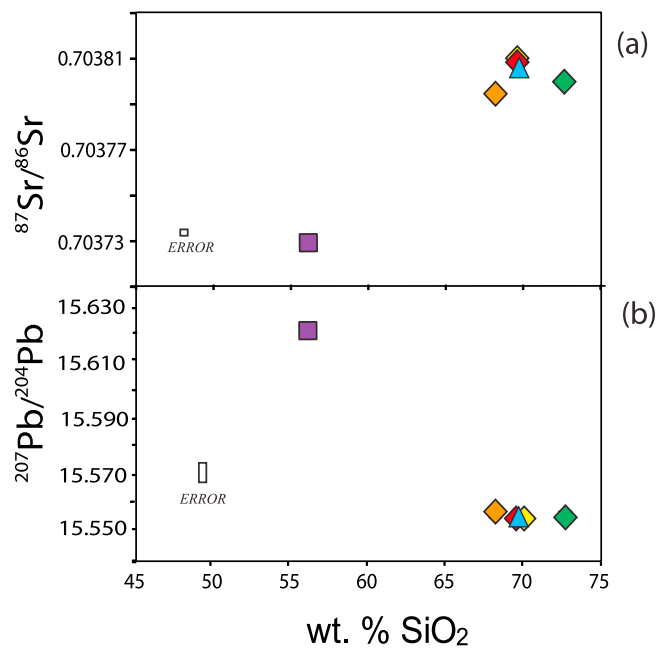


Figure 8. Weight % SiO_2 versus (a) $^{87}\text{Sr}/^{86}\text{Sr}$ and (b) $^{207}\text{Pb}/^{204}\text{Pb}$ for the Ilopango samples.

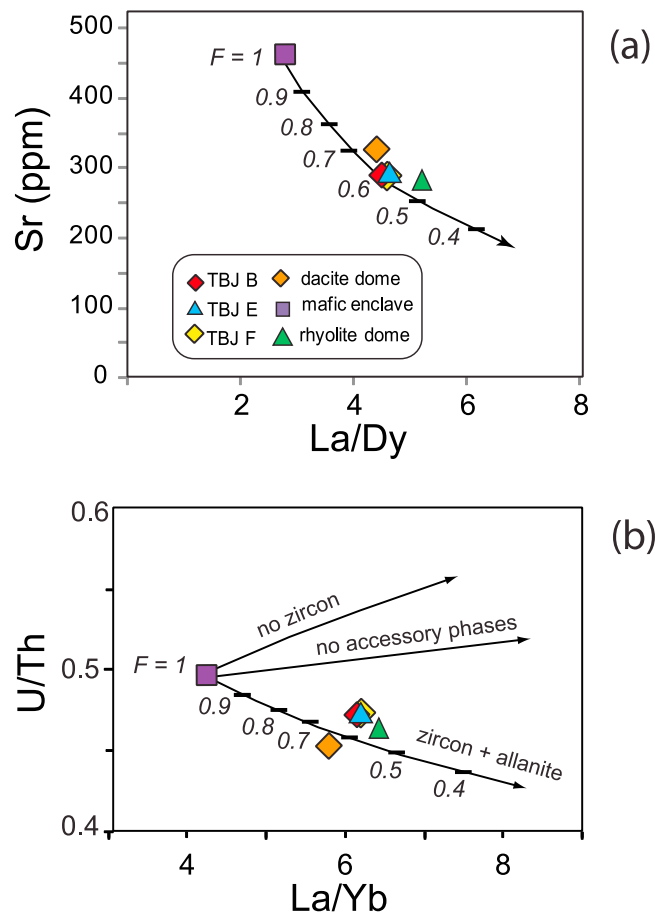


Figure 9. (a) La/Dy versus ppm Sr for the Ilopango samples showing the same fractional crystallization modeled curve used in Figure 4a. F = the proportion of melt remaining. This model shows that the range of values can be reproduced using 30–50% crystallization. (b) La/Yb versus U/Th showing the effects of accessory phase fractionation. The top curve shows the modeled curve with no accessory zircon in the mineral assemblage, only allanite and apatite. The middle curve was modeled using no accessory phases, and the curve that best fits the data requires both zircon and allanite, and to a lesser extent, apatite.

Smith, 2010] (Figure 11). Collectively, the data show a correlation between position along the arc and ($^{230}\text{Th}/^{232}\text{Th}$). The highest ($^{230}\text{Th}/^{232}\text{Th}$) values are reported from rocks in Nicaragua, and these exceptionally high values (perhaps the highest in the world) are attributed to the high U/Th of the slab fluids and aging of the mantle source [Reagan *et al.*, 1994; Thomas *et al.*, 2002]. Values decrease to the north of Nicaragua, and the Ilopango rocks have an average ($^{230}\text{Th}/^{232}\text{Th}$) value of 1.52, which is within the range of other published data for El Salvador (Figure 11).

[18] In terms of ($^{230}\text{Th}/^{238}\text{U}$), most Central American lavas have values typically within 10% of equilibrium; the greatest observed ^{238}U excesses are about 15% at Cerro Negro. On the other hand, ^{230}Th excesses are typically of greater magnitude, and a significant proportion of the basalts and basaltic

andesites have ^{230}Th excesses rather than ^{238}U excesses (e.g., Concepción and high-Nb Nejapa lavas in Nicaragua [Reagan *et al.*, 1994]). Excess ^{230}Th is particularly pronounced in mafic lavas from Central Costa Rica (e.g., Turrialba, Irazu) that have parental lavas generated by low-degrees of mantle melting in the presence of garnet and little slab flux [e.g., Reagan and Gill, 1989]. ^{230}Th excesses in basalts from Nicaragua have been attributed to melting of hornblende-bearing crystal cumulates [Reagan *et al.*, 1994], and Walker *et al.* [2007] concluded that ^{230}Th excesses in mafic rocks from Guatemala are the result of crustal contamination. Thomas *et al.* [2002] explained ^{230}Th excesses in Nicaragua and Costa Rica using a continuous flux-growth melting model. The 20% ^{226}Ra excess (with respect to ^{230}Th) in the Ilopango 1880 basaltic andesite enclave is similar in scale to those found in lavas from Costa Rica [Thomas *et al.*, 2002] and

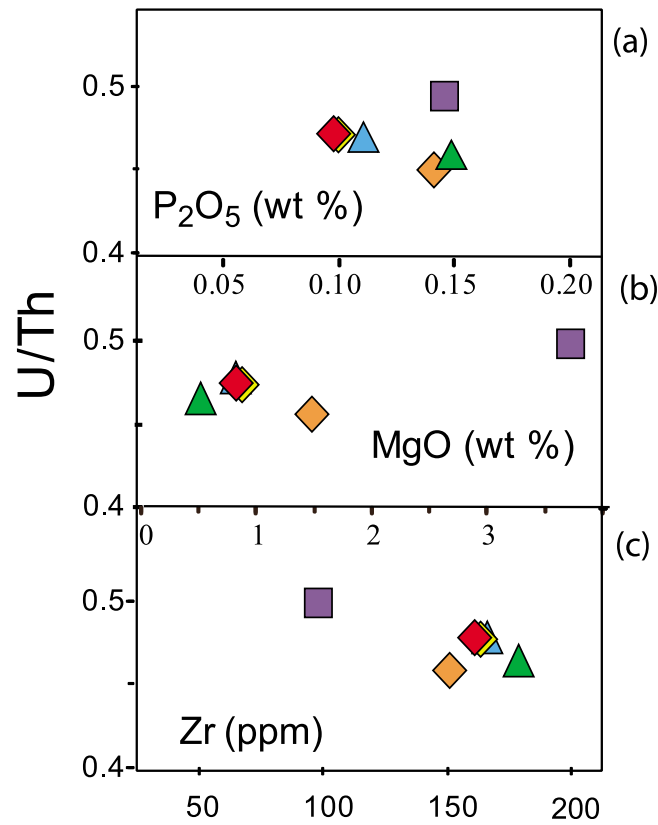


Figure 10. Graphs of weight % (a) P_2O_5 and (b) MgO and (c) ppm Zr, versus U/Th for the Ilopango samples. These data show that there is no correlation between U/Th and MgO . There is a slight negative correlation with ppm Zr.

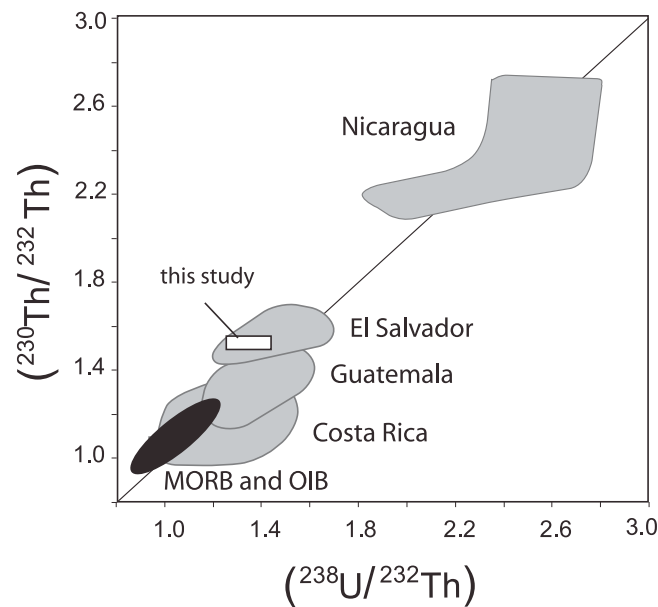


Figure 11. Equiline diagram showing U-series data for the CAVA, with the Ilopango data superimposed on the field for El Salvador. Fields are from Walker *et al.* [2007].

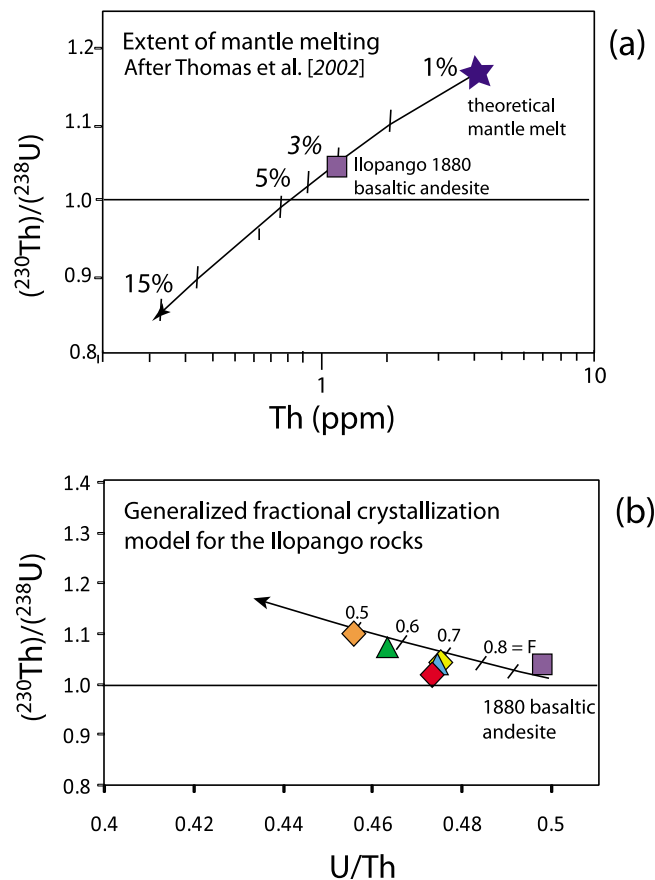


Figure 12. (a) Model curve from *Thomas et al.* [2002], showing the average extent of mantle melting and the effect on the $(^{230}\text{Th}/^{238}\text{U})$ and Th ppm. The starting composition is a theoretical 1% partial melt of garnet-bearing enriched mantle similar to that beneath Costa Rica (blue symbol). The Ilopango basaltic andesite (red symbol) value is consistent with an extent of melting of 3%. (b) Numerical model curve of fractional crystallization, using the same mineral assemblages and bulk D value as Figures 4, 7, and 9. The TBJ data seem to project back to an actual parental magma composition either has a lower $(^{230}\text{Th}/^{238}\text{U})$ and/or U/Th than the basaltic andesite.

Guatemala [*Walker et al.*, 2007], unlike the 50–250% ^{226}Ra excesses found in the strongly subduction fluid affected lavas from Nicaragua [*Reagan et al.*, 1994; *Thomas et al.*, 2002]. The ^{230}Th and ^{226}Ra excesses in the Ilopango samples are most consistent with the flux-ingrowth melting model of *Thomas et al.* [2002], which simultaneously explains the 4% ^{230}Th excesses and the 20% ^{226}Ra excesses in the Ilopango basaltic andesite using an average extent of melting of 3–4% and a mantle composition similar to that beneath Nicaragua (Figure 12a).

6.3. U-Series Evidence for Magma Differentiation at Ilopango

[19] If, like the basaltic andesite, the ^{230}Th excesses of the TBJ dacites are inherited from the mantle, this would require that the time elapsed since mantle melting, including ascent and differentiation

to dacite is less than 5,000 years; a short time for continental arcs [*Turner et al.*, 2000]. It seems more likely that the increase in $(^{230}\text{Th}/^{238}\text{U})$ from the basaltic andesite to the 1880 dacite and rhyolite domes is more likely a differentiation effect. Most of the compositional differences between the basaltic andesite and the TBJ tephras can be modeled using crystal fractionation of accessory phases (Figures 9b and 12b). It has been shown that crystallization of accessory phases allanite, apatite and monazite can sequester Th and create significant disequilibria [*Schmitt*, 2011; *Garrison et al.*, 2006], but zircon is the only accessory mineral capable of sequestering significant U to create ^{230}Th excesses, perhaps with the exception of magnetite. The TBJ mineral separate data show that magnetite from all three units have (^{238}U) excesses of 4%. The high $(^{238}\text{U}/^{230}\text{Th})$ of 2.7 in the TBJ-F amphibole mineral separate (Figure 6b) is likely the result of zircon inclusions. The correlation between decreasing

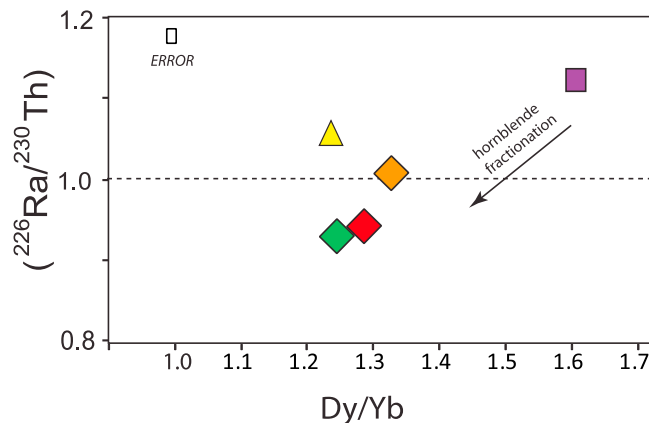


Figure 13. $(^{226}\text{Ra}/^{230}\text{Th})$ data versus Dy/Yb for the Ilopango samples. The black arrow shows the effect of hornblende fractionation on Dy/Yb.

magnitude of the ^{226}Ra excess and weight percent SiO_2 (Figure 7b) strongly suggests that the ^{226}Ra variation is related to crystallization of a Ra-bearing phase within the last few thousand years, although aging might have equilibrated the $(^{226}\text{Ra}/^{230}\text{Th})$ values for some dacites. The minerals that provide the greatest leverage over $(^{226}\text{Ra})/(^{230}\text{Th})$ are K-bearing phases, specifically amphibole and the alkali feldspars [Sims *et al.*, 2002] including anorthoclase [Cooper and Donnelly, 2008; Reagan *et al.*, 1994]. Ra partitions preferentially into these minerals, and less effectively into plagioclase [Fabbrizio *et al.*, 2009]. The composition of the Ilopango feldspar (Table S1) ranges $\text{An}_{49}\text{-An}_{53}$ with $\text{K}_2\text{O} < 0.3$ wt %, and this composition of plagioclase (labradorite) does not significantly partition Ra [Fabbrizio *et al.*, 2009, 2010]. On the other hand, elastic strain models suggest that amphibole does preferentially retain Ra relative to Th [Feineman and DePaolo, 2003]. Amphibole also retains MREE, and fractionation is commonly represented as a decrease in Dy/Yb during differentiation. There is a positive correlation between $(^{226}\text{Ra})/(^{230}\text{Th})$ and Dy/Yb in the Ilopango samples (Figure 13), and one way to explain the Ra-Ba-Th trend is fractionation from basaltic andesite to dacite involving a hornblende-rich assemblage that lowers Dy/Yb and $(^{226}\text{Ra})/(^{230}\text{Th})$. In the Ilopango basaltic andesite Dy/Yb = 1.6, however in the dacite, rhyolite and TBJ dacites Dy/Yb ranges from 1.35 to 1.22 (Figure 13). This 9% decrease correlates with a concomitant decrease in $(^{226}\text{Ra}/^{230}\text{Th})$. We propose that the $(^{238}\text{U}/^{232}\text{Th})$ and $(^{226}\text{Ra}/^{230}\text{Th})$ variation in the Ilopango dacites reflects crystallization of hornblende, followed by accessory phase fractionation of allanite and zircon in the magma chamber prior to eruption of the TBJ dacites (model curves shown on Figures 7a, 9b, and 12b). This

model is also consistent with the variations in REE patterns for Ilopango tephra (Figure 4a).

6.4. U-Series Evidence for Magma Storage Times at Ilopango Caldera

[20] The Ilopango whole-rock data form a sub-horizontal array on the equiline diagram (Figure 6) that is consistent with a <10,000 year time frame since U-Th fractionation for all the samples, including the rhyolite dome, which, on the basis of these data is likely to have the same eruption age as the 1880 dacite domes. The mineral separate data yield isochrons that were calculated using age-corrected data for the TBJ-B, E and F units. By using age-corrected data, the calculated isochron ages represent the time elapsed between the average age of mineral growth and magma eruption. This reflects the average storage time of the TBJ dacite, assuming that the crystals grew in conjunction with crystal fractionation. The averaged isochron ages for units E, F and B, using the York regression [Mahon, 1996] is <4,000 years, however given the considerable scatter in the $(^{230}\text{Th}/^{232}\text{Th})$ values, it is most reasonable to interpret the array as being consistent with fractionation from basaltic andesite to dacite in less than 8,000 years. This a short enough time span to preserve $(^{226}\text{Ra})/(^{230}\text{Th})$ disequilibrium in some samples (TBJ-B and the rhyolite dome), although other dacites had a long enough residence time in the crust for ^{226}Ra to attain equilibrium with ^{230}Th . This is quite remarkable considering that this timeframe must allow for the generation of 70 km^3 of dacite. Using the calculated 50% crystallization from the basaltic andesite, this equates to a continuous crystallization rate on the order of $5.0 \times 10^{-3} \text{ yr}^{-1}$,

similar to trachytes from the Azores [*Snyder et al.*, 2007].

[21] Several recent studies have raised the issue of mixing among crystal populations that may mask the true isochrons in volcanic rocks [*Fabrizio et al.*, 2009; *Cooper et al.*, 2003; *Cooper and Donnelly*, 2008]. These studies demonstrate that mixing of multiple crystal populations, or the presence of melt inclusions in minerals can yield a linear array that is actually a mixing line. Indeed, the three populations of plagioclase crystals in the TBJ units cannot have an entirely shared history. We point out, however that the mineral assemblages among the TBJ tephras have identical ($^{230}\text{Th}/^{232}\text{Th}$), whereas scavenged minerals with significant concentrations of Th and U concentrations, if they are significantly older than the Ilopango dacite affect the nearly horizontal U-Th array. This further illustrates the lack of evidence for the involvement of a significant volume of older magmas or crystals in the TBJ eruption. The three Ilopango units (B, E, F) could represent mixtures of unsampled end-member magmas since they all shared the same magma reservoir. Nevertheless, the isotope and trace element data indicate that the magmas are cogenetic, and cogenetic magmas that define a horizontal isochron must be essentially “zero-aged” even if they mix with each other. Similarly, melt inclusions can also have a large impact on the isotope compositions of the crystals because glass inclusions may contain the majority of U, Ra and Th in the plagioclase and amphibole. At Ilopango, however, the impact of contamination by glass inclusions is likely to be low for these samples, since none of the mineral separates have ($^{230}\text{Th}/^{232}\text{Th}$) above the whole rock value of 1.5, and the glass composition is similar to the whole rock values.

[22] In the broader context of magmagenesis, our results are consistent with studies that show fractional crystallization and melt extraction to be the primary mechanisms for rhyolite formation in arc systems [*Bachmann and Bergantz*, 2003, 2004; *Brophy*, 1991]. Calculated segregation times for the Ilopango dacites, using models of hindered settling and filter pressing (compaction) from *Bachmann and Bergantz* [2004] range from 10^4 - 10^6 years for large magmatic systems. Our results suggest that crystal fractionation at Ilopango is at the short end of this range. The previous significant eruption from Ilopango Caldera, the TB-2 eruption is dated at 15,000 years old, and the TB-4 eruption is dated at 36,000 years. On the basis of these ages, it appears that the repose time between eruptions at Ilopango Caldera is on the order of 15–20 ka. Our U-series data are consistent with an average crustal

residence time for magmas involved with the TBJ eruption that is well within this time-frame.

[23] Dacite and rhyolite lavas are commonly believed to represent the degassed residual magma after large eruptions [*Streck and Grunder*, 2007], and the Cerros Quemados dacite domes are consistent with other examples of post-caldera magmatism (e.g., Incapillo Caldera [*Goss et al.*, 2009], Valles Caldera [*Wolff and Gardner*, 1995], and Mount St Helens [*Rowe et al.*, 2008]). In some cases, dome lavas are believed to represent magma that was co-genetic with the primary eruption (Long Valley Caldera [*Heumann and Davies*, 1997; *Higgins and Meilleur*, 2009]); in other cases there is evidence to indicate a component of juvenile magma (Yellowstone [*Vazquez et al.*, 2009]). At Ilopango caldera, the basaltic enclaves clearly postdate the development of the TBJ dacites, and it is likely that input of this juvenile magma into the system triggered the 1880 eruption. The rhyolite dome (Il Pat), which must postdate the TBJ eruption, has a composition indicating that it was generated by crystal fractionation of residual TBJ magma (Figures 7 and 9a).

[24] In terms of timescales, repose times between rhyolite eruptions range from 10^5 - 10^6 years for large caldera systems (i.e., Yellowstone [*Reid et al.*, 1997] and Toba [*Vazquez and Reid*, 2004; *de Silva*, 2008]), to 10^3 years for smaller systems (e.g., Okataina Volcanic Complex [*Klemetti et al.*, 2011] and Cotopaxi Volcano [*Hall and Mothes*, 2008; *Garrison et al.*, 2011]). On the basis of tephra chronology, repose times have been established for many calderas in the CAVA (e.g., Chiltepe, Coatepeque, Apoyo, Los Chocoyos, Apoyeque [*Kutterolf et al.*, 2007, 2008a, 2008b]), however the magma residence times for these systems are unknown. In fact, despite the large number of explosive rhyolite calderas in the CAVA there are surprisingly few studies on magma residence times. Future studies of residence times in other CAVA caldera systems may be useful to assess if rapid differentiation and short storage times are typical of other Central American calderas.

7. Conclusions

[25] The U-series and long-lived isotope data from TBJ dacites of Ilopango Caldera indicate that neither the mineral isochrons nor whole rock U-series data record a protracted storage time for the Ilopango TBJ dacite. Crustal residence times of magmas at Ilopango are on the order of 10^3 - 10^4 years, and magma production rate at Ilopango must be on the order of

10^{-4} km³/km/yr in order to explain the U-series disequilibria in this system. The $(^{238}\text{U})/(^{230}\text{Th})$ variation in the Ilopango TBJ dacites is related to accessory phase crystallization during differentiation, and the $(^{226}\text{Ra})/(^{230}\text{Th})$ variation is related to amphibole fractionation. The 1880 eruption was likely triggered by an intrusion of an isotopically distinct basaltic andesite into the base of the system. In fact, the eruption of rhyolite and dacite domes in Lago Ilopango illustrates that magmatic activity is ongoing, and that this rapidly developing system has a robust supply of magma. However, the 15–20 ka repose time between large eruptions, coupled with the observation that the most recent eruption was of a degassed, relatively mafic dacite suggests that a large body of more differentiated dacite does not presently exist beneath Ilopango Caldera.

Acknowledgments

[26] We thank NSF for funding Garrison under the MARGINS post-doctoral fellowship program (OCE 0405262). We also thank Shan deSilva, Tom Vogel and the editor James Tyburczy for thoughtful reviews that strengthened our final manuscript. We are grateful to D. Peate and M. Wortel at the University of Iowa, as well as L. Ball, J. Blusztajn and Dave Schneider at Woods Hole Oceanographic Institute for assistance with analyses. We also thank the lab staff at MSU for conducting the XRF/ICP analyses, and Frank Kyte and UCLA for help with the electron microprobe analyses. We are also grateful to the staff at SNET (Servicio Nacional de Estudios Territoriales) in El Salvador for their help with sample locations and field work.

References

- Bachmann, O., and G. W. Bergantz (2003), Rejuvenation of the Fish Canyon magma body: A window into the evolution of large-volume silicic magma systems, *Geology*, *31*, 789–792, doi:10.1130/G19764.1.
- Bachmann, O., and G. W. Bergantz (2004), On the origin of crystal-poor rhyolites: extracted from batholithic crystal mushes, *J. Petrol.*, *45*, 1565–1582, doi:10.1093/ptrology/egh019.
- Ball, L. A., K. W. W. Sims, and J. Schwieters (2008), Measurement of $^{234}\text{U}/^{238}\text{U}$ and $^{230}\text{Th}/^{232}\text{Th}$ in volcanic rocks using the Neptune PIMMS, *J. Anal. At. Spectr.*, *23*, 173–180, doi:10.1039/b703193a.
- Bice, D. C. (1985), Quaternary volcanic stratigraphy of Managua, Nicaragua: Correlation and source assignment for multiple overlapping Plinian deposits, *Geol. Soc. Am. Bull.*, *96*, 553–566, doi:10.1130/0016-7606(1985)96<553:QVSOMN>2.0.CO;2.
- Brophy, J. G. (1991), Composition gaps, critical crystallinity, and fractional crystallization in orogenic (calc-alkaline) magmatic systems, *Contrib. Mineral. Petrol.*, *109*, 173–182, doi:10.1007/BF00306477.
- Carey, S., and H. Sigurdsson (2000), Grain size of Miocene ash volcanic layers from sites 998, 999 and 1000; Implications for source areas and dispersal, *Proc. Ocean Drill. Program Sci. Results*, *165*, 315–326.
- Carr, M. J. (1984), Symmetrical and segmented variation of physical and geochemical characteristics of the Central American volcanic front, *J. Volcanol. Geotherm. Res.*, *20*(3–4), 231–252, doi:10.1016/0377-0273(84)90041-6.
- Carr, M. J., M. D. Feigenson, and E. A. Bennett (1990), Incompatible element and isotopic evidence for tectonic control of source mixing and melt extraction along the Central American arc, *Contrib. Mineral. Petrol.*, *105*(4), 369–380, doi:10.1007/BF00286825.
- Carr, M. J., M. D. Feigenson, L. C. Patino, and J. A. Walker (2003), Volcanism and geochemistry in Central America: Progress and problems, in *Inside the Subduction Factory*, *Geophys. Mon. Ser.*, vol. 138, edited by J. Eiler, pp. 153–179, AGU, Washington, D. C.
- Clark, S. K., M. K. Reagan, and T. Plank (1998), Trace element and U-series systematics for 1963–1965 tephra from Irazu Volcano, Costa Rica: Implications for magma generation processes and transit times, *Geochim. Cosmochim. Acta*, *62*, 2689–2699.
- Cooper, K. M., and C. T. Donnelly (2008), ^{238}U – ^{230}Th – ^{226}Ra disequilibria in dacite and plagioclase from the 2004–2005 eruption of Mount St. Helens, in *A Volcano Rekindled: The Renewed Eruption of Mount St. Helens, 2004–2006*, edited by D. R. Sherrod, W. E. Scott, and P. H. Stauffer, pp. 827–846, U.S. Geol. Surv., Reston, Va.
- Cooper, K., S. J. Goldstein, K. W. W. Sims, and M. T. Murrell (2003), Uranium-series chronology of Gorda Ridge volcanism: New evidence from the 1996 eruption, *Earth Planet. Sci. Lett.*, *206*, 459–475, doi:10.1016/S0012-821X(02)01083-X.
- Davidson, J. P. (1996), Deciphering mangle and crustal signatures in subduction zone magmatism, in *Subduction, Top to Bottom*, *Geophys. Monogr. Ser.*, vol. 96, edited by E. Bebout et al., pp. 251–262, AGU, Washington, D. C., doi:10.1029/GM096p0251.
- Davidson, J. P., S. P. Turner, H. Handley, C. Macpherson, and A. Dosseto (2007), Amphibole “sponge” in arc crust?, *Geology*, *35*, 787–790, doi:10.1130/G23637A.1.
- Deering, G., J. W. Cole, and T. A. Vogel (2008), A rhyolite compositional continuum governed by lower crustal source conditions in the Taupo Volcanic Zone, New Zealand, *J. Petrol.*, *49*(12), 2245–2276, doi:10.1093/ptrology/egn067.
- DeMets, C. (2001), A new estimate for present-day Cocos-Caribbean plate motion: Implications for slip along the Central American volcanic arc, *Geophys. Res. Lett.*, *28*, 4043–4046, doi:10.1029/2001GL013518.
- DeMets, C., R. G. Gordon, D. F. Argus, and S. Stein (1990), Current plate motions, *Geophys. J. Int.*, *101*, 425–478, doi:10.1111/j.1365-246X.1990.tb06579.x.
- de Silva, S. (2008), Arc magmatism, calderas, and supervolcanoes, *Geology*, *36*, 671–672, doi:10.1130/focus082008.1.
- Dull, R., J. Southon, and P. Sheets (2001), Volcanism, ecology and culture: A reassessment of the volcan Ilopango TBJ eruption in the southern Maya realm, *Lat. Am. Antiq.*, *12*, 25–44, doi:10.2307/971755.
- Fabbrizio, A., M. W. Schmidt, G. Detlef, and J. Eikenberg (2009), Experimental determination of Ra mineral/melt partitioning for feldspars and ^{226}Ra -disequilibrium crystallization ages of plagioclase and alkali-feldspar, *Earth Planet. Sci. Lett.*, *280*, 137–148, doi:10.1016/j.epsl.2009.01.022.
- Fabbrizio, A., M. W. Schmidt, G. Detlef, and J. Eikenberg (2010), Ra-partitioning between phlogopite and silicate melt and $^{226}\text{Ra}/\text{Ba}$ – $^{230}\text{Th}/\text{Ba}$ isochrons, *Lithos*, *114*, 121–131, doi:10.1016/j.lithos.2009.08.004.

- Feigenson, M. D., and M. J. Carr (1986), Positively correlated Nd and Sr isotope ratios of lavas from the Central American volcanic front, *Geology*, *14*(1), 79–82, doi:10.1130/0091-7613(1986)14<79:PCNASI>2.0.CO;2.
- Feigenson, M. D., and M. J. Carr (1993), The source of Central American lavas: Inferences from geochemical inverse modeling, *Contrib. Mineral. Petrol.*, *113*, 226–235, doi:10.1007/BF00283230.
- Feineman, M. D., and D. J. DePaolo (2003), Steady-state $^{226}\text{Ra}/^{230}\text{Th}$ disequilibrium in mantle minerals: Implications for melt transport rates in island arcs, *Earth Planet. Sci. Lett.*, *215*, 339–355, doi:10.1016/S0012-821X(03)00454-0.
- Garrison, J. M., J. P. Davidson, M. Reid, and S. P. Turner (2006), Source versus differentiation controls on U-series disequilibria: Insights from Cotopaxi Volcano, Ecuador, *Earth Planet. Sci. Lett.*, *244*, 548–565, doi:10.1016/j.epsl.2006.02.013.
- Garrison, J. M., J. P. Davidson, M. Hall, and P. Mothes (2011), Geochemistry and petrology of the most recent deposits from Cotopaxi Volcano, Northern Volcanic Zone, Ecuador, *J. Petrol.*, *52*, 1–38.
- Geldmacher, J., K. Hoernle, P. VanDenBogaard, F. Hauff, and A. Klugel (2008), Age and geochemistry of the Central American forearc basement (DSDP Leg 67 and 84), Insights into Mesozoic arc volcanism and seamount accretion on the fringe of the Caribbean LIP, *J. Petrol.*, *12*, 643–698.
- Gill, J. B. (1981), *Orogenic Andesites and Plate Tectonics*, *Miner. and Rocks*, vol. 16, 390 pp., Springer, Berlin, doi:10.1007/978-3-642-68012-0.
- Goss, A. R., S. M. Kay, C. Mpodozis, and B. S. Singer (2009), The Incapillo Caldera and Dome Complex (~28° S, Central Andes): A stranded magma chamber over a dying arc, *J. Volcanol. Geotherm. Res.*, *184*, 389–404, doi:10.1016/j.jvolgeores.2009.05.005.
- Hall, M., and P. Mothes (2008), The rhyolitic-andesitic eruptive history of Cotopaxi volcano, Ecuador, *Bull. Volcanol.*, *70*, 675–702, doi:10.1007/s00445-007-0161-2.
- Hawkesworth, C. J., S. P. Turner, F. McDermott, D. W. Peate, and P. van Calsteren (1997), U-Th isotopes in arc magmas: Implications for element transfer from the subducted crust, *Science*, *276*, 551–555, doi:10.1126/science.276.5312.551.
- Herrstrom, E. A., and M. K. Reagan (1995), Variations in lava composition associated with flow of asthenosphere beneath southern Central America, *Geology*, *23*, 617–620, doi:10.1130/0091-7613(1995)023<0617:VILCAW>2.3.CO;2.
- Heumann, A., and G. R. Davies (1997), Isotopic and chemical evolution of the post-caldera rhyolite system at Long Valley, California, *J. Petrol.*, *38*, 1661–1678, doi:10.1093/ptroj/38.12.1661.
- Higgins, M. D., and D. Meilleur (2009), Development and emplacement of the Inyo Domes Magmatic Suite, California: Evidence from geological, textural (CSD) and geochemical observations of ash and lava, *J. Volcanol. Geotherm. Res.*, *186*, 280–292, doi:10.1016/j.jvolgeores.2009.07.004.
- Jicha, B. R., and K. E. Smith (2010), Crustal assimilation no match for slab fluids beneath Volcán de Santa María, Guatemala, *Geology*, *38*(9), 859–862, doi:10.1130/G31062.1.
- Johnson, D. M., P. R. Hooper, and R. M. Conrey (1999), XRF analysis of rocks and minerals for major and trace elements on a single low dilution Li-tetraborate fused bead, *Adv. X Ray Anal.*, *41*, 843–867.
- Jordan, B. R., et al. (2006), Geochemical correlation of Caribbean Sea tephra layers with ignimbrites in Central America, in *Neogene-Quaternary Continental Margin Volcanism: A Perspective from Mexico*, edited by C. Siebe, J. L. Macias, and G. J. Aguirre-Díaz, *Spec. Pap. Geol. Soc. Am.*, *402*, 161–194.
- Klemetti, E. W., C. D. Deering, K. M. Cooper, and S. M. Roeske (2011), Magmatic perturbations in the Okataina Volcanic Complex, New Zealand at thousand-year timescales recorded in single zircon crystals, *Earth Planet. Sci. Lett.*, *305*, 185–194, doi:10.1016/j.epsl.2011.02.054.
- Knaak, C., S. B. Cornelius, and P. R. Hooper (1994), Trace element analyses of rocks and minerals by ICP-MS, technical note, GeoAnal. Lab., Wash. State Univ., Pullman.
- Kutterolf, S., A. Freundt, W. Peréz, W. Wehrmann, and U. Schmincke (2007), LatePleistocene to Holocene temporal succession and magnitudes of highly explosive volcanic eruptions in west-central Nicaragua, *J. Volcanol. Geotherm. Res.*, *163*, 55–82, doi:10.1016/j.jvolgeores.2007.02.006.
- Kutterolf, S., A. Freundt, W. Peréz, T. Mörz, U. Schacht, H. Wehrmann, and H.-U. Schmincke (2008a), Pacific offshore record of plinian arc volcanism in Central America: 1. Along-arc correlations, *Geochem. Geophys. Geosyst.*, *9*, Q02S01, doi:10.1029/2007GC001631.
- Kutterolf, S., A. Freundt, and W. Peréz (2008b), Pacific offshore record of plinian arc volcanism in Central America: 2. Tephra volumes and erupted masses, *Geochem. Geophys. Geosyst.*, *9*, Q02S02, doi:10.1029/2007GC001791.
- Le Maitre, R. W., et al. (1989), *A Classification of Igneous Rocks and a Glossary of Terms*, 342 pp., Blackwell, Oxford, U. K.
- Lexa, J., et al. (2011), Geology and volcanic evolution in the southern part of the San Salvador metropolitan area, *J. Geosci.*, *56*, 105–140.
- MacKenzie, L. S., G. A. Abers, S. Rondenay, and K. M. Fischer (2010), Imaging a steeply dipping subducting slab in southern Central America, *Earth Planet. Sci. Lett.*, *296*, 459–468, doi:10.1016/j.epsl.2010.05.033.
- Mahon, K. I. (1996), The New “York” regression: Application of an improved statistical method to geochemistry, *Int. Geol. Rev.*, *38*, 293–303, doi:10.1080/00206819709465336.
- Mehring, P. J. J., A. M. Sarna-Wojcickib, L. K. Wollwagec, and P. Sheets (2005), Age and extent of the Ilopango TBJ Tephra inferred from a Holocene chronostratigraphic reference section, Lago De Yojoa, Honduras, *Quat. Res.*, *63*, 199–205, doi:10.1016/j.yqres.2004.09.011.
- Reagan, M. K., and J. B. Gill (1989), Coexisting calcalkaline and high-Nb basalts from Turrialba volcano, Costa Rica: Implications for residual titanates in arc magma sources, *J. Geophys. Res.*, *94*, 4619–4633, doi:10.1029/JB094iB04p04619.
- Reagan, M. K., J. D. Morris, E. A. Herrstrom, and M. T. Murrell (1994), Uranium series and beryllium isotope evidence for an extended history of subduction modification of the mantle below Nicaragua, *Geochim. Cosmochim. Acta*, *58*, 4199–4212, doi:10.1016/0016-7037(94)90273-9.
- Reid, M. R., C. D. Coath, M. T. Harrison, and K. D. McKeegan (1997), Prolonged residence times for the youngest rhyolites associated with Long Valley Caldera: ^{230}Th - ^{238}U ion microprobe dating of young zircons, *Earth Planet. Sci. Lett.*, *150*, 27–39.
- Rose, W. I., et al. (1979), Geochemistry of the Los Chocoyos ash, Guatemala, in *Ash Flow Tuffs*, edited by W. Elston and C. Chapin, *Spec. Pap. Geol. Soc. Am.*, *180*, 87–99.
- Rose, W. I., F. M. Conway, C. R. Pullinger, A. Deino, and W. C. McIntosh (1999), An improved age framework for late Quaternary silicic eruptions in northern Central America, *Bull. Volcanol.*, *61*, 106–120, doi:10.1007/s004450050266.
- Rowe, M. C., C. R. Thorber, and A. J. R. Kent (2008), Identification and evolution of the juvenile component in 2004–2005 Mount St. Helens ash, in *A Volcano Rekindled: The Renewed Eruption of Mount St. Helens, 2004–2006*, edited by D. R.

- Sherrod, W. E. Scott, and P. H. Stauffer, pp. 629–646, U.S. Geological Survey, Reston, Va.
- Schmidt, M. W., A. Dardon, R. Vannucci, and R. Chazo (2004), The dependence of Nb and Ta rutile-melt partitioning on melt composition and Nb/Ta fractionation during subduction processes, *Earth Planet. Sci. Lett.*, *226*, 415–432, doi:10.1016/j.epsl.2004.08.010.
- Schmitt, A. K. (2011), Uranium series accessory crystal dating of magmatic processes, *Annu. Rev. Earth Planet. Sci.*, *39*, 321–349, doi:10.1146/annurev-earth-040610-133330.
- Sigurdsson, H., R. M. Kelley, S. Carey, T. Bralower, and J. King (2000), History of circum-Caribbean explosive volcanism: $^{40}\text{Ar}/^{39}\text{Ar}$ dating of tephra layers, *Proc. Ocean Drill. Program Sci. Results*, *165*, 299–314.
- Sims, K. W. W., et al. (2002), Chemical and isotopic constraints on the generation and transport of melt beneath the East Pacific Rise, *Geochim. Cosmochim. Acta*, *66*(19), 3481–3504, doi:10.1016/S0016-7037(02)00909-2.
- Sims, K. W. W., J. Blichert-Toft, P. R. Kyle, S. Pichat, J. Blusztajn, P. J. Kelly, L. A. Ball, and G. D. Layne (2008a), A Sr, Nd, Hf, and Pb isotope perspective on the genesis and long-term evolution of alkaline magmas from Erebus volcano, Antarctica, Special volume on Mt Erebus, *J. Volcanol. Geotherm. Res.*, *177*, 606–618, doi:10.1016/j.jvolgeores.2007.08.006.
- Sims, K. W. W., S. R. Hart, M. K. Reagan, J. Blusztajn, H. Staudigel, R. A. Sohn, G. D. Layne, L. A. Ball, and J. Andrews (2008b), ^{238}U – ^{230}Th – ^{226}Ra – ^{210}Pb – ^{210}Po , ^{232}Th – ^{228}Ra and ^{235}U – ^{231}Pa constraints on the ages and petrogenesis of Vailulu'u and Malumalu Lavas, Samoa, *Geochem. Geophys. Geosyst.*, *9*, Q04003, doi:10.1029/2007GC001651.
- Sims, K. W. W., et al. (2008c), An inter-laboratory assessment of the thorium isotopic composition of synthetic and rock reference materials, *Geostand. Anal. Res.*, *32*(1), 65–91, doi:10.1111/j.1751-908X.2008.00870.x.
- Snyder, D. R., E. Widom, A. J. Pietruszka, R. W. Carlson, and H.-U. Schmincke (2007), Time scales of formation of zoned magma chambers: U-series disequilibria in the Fogo A and 1563 A.D. trachyte deposits, São Miguel, Azores, *Chem. Geol.*, *239*, 138–155, doi:10.1016/j.chemgeo.2007.01.002.
- Streck, M. J., and A. Grunder (2007), Phenocryst-poor rhyolites of bimodal, tholeiitic provinces: The Rattlesnake Tuff and implications for mush extraction models, *Bull. Volcanol.*, *70*, 385–401.
- Sun, S. S., and W. F. McDonough (1989), Chemical and isotopic systematics of oceanarc basalts: Implications for mantle composition and processes, *Geol. Soc. London Spec. Publ.*, *42*, 313–345.
- Sussman, D. (1985), Apoyo caldera, Nicaragua: A major quaternary silicic eruptive center, *J. Volcanol. Geotherm. Res.*, *24*(3–4), 249–282, doi:10.1016/0377-0273(85)90072-1.
- Tepley, F. J., III, and C. C. Lundstrom (2006), U-Th-Ra disequilibria and the time scale of fluid transfer and andesite differentiation at Arenal Volcano, Costa Rica (1968–2003), *J. Volcanol. Geotherm. Res.*, *157*, 147–165, doi:10.1016/j.jvolgeores.2006.03.038.
- Thomas, R. B., et al. (2002), ($^{231}\text{Pa}/^{235}\text{U}$)-($^{230}\text{Th}/^{238}\text{U}$) of young mafic volcanic rocks from Nicaragua and Costa Rica and the influence of flux melting on U-series systematics of arc lavas, *Geochim. Cosmochim. Acta*, *66*(24), 4287–4309, doi:10.1016/S0016-7037(02)00993-6.
- Tiepolo, M., P. Bottazzi, S. F. Foley, R. Oberti, R. Vannucci, and A. Zanetti (2001), Fractionation of Nb and Ta from Zr and Hf at mantle depths: The role of titanian pargasite and kaersutite, *J. Petrol.*, *42*, 221–232, doi:10.1093/petrology/42.1.221.
- Todt, W., and R. A. Cliff (1996), Evaluation of a ^{202}Pb – ^{205}Pb double spike for high-precision lead isotope analysis, in *Earth Processes: Reading the Isotope Code*, *Geophys. Monogr. Ser.*, vol. 95, edited by S. R. Hart and A. Basu, pp. 429–437, AGU, Washington, D. C.
- Turner, S. P., R. M. George, P. J. Evans, C. J. Hawkesworth, and G. F. Zellmer (2000), Timescales of magma formation, ascent and storage beneath subduction-zone volcanoes, *Philos. Trans. R. Soc. London*, *358*, 1443–1464, doi:10.1098/rsta.2000.0598.
- Vazquez, J. A., and M. R. Reid (2004), Probing the accumulation history of the voluminous Toba magma, *Science*, *305*, 991–994, doi:10.1126/science.1096994.
- Vazquez, J. A., S. F. Kyriazis, M. R. Reid, R. C. Sehler, and F. C. Ramos (2009), Thermochemical evolution of young rhyolites at Yellowstone: Evidence for a cooling but periodically replenished postcaldera magma reservoir, *J. Volcanol. Geotherm. Res.*, *201*, 45–87.
- Vogel, T. A., et al. (2006), Origin of silicic magmas along the Central American volcanic front: Genetic relationship to mafic melts, *J. Volcanol. Geotherm. Res.*, *156*, 217–228, doi:10.1016/j.jvolgeores.2006.03.002.
- Walker, J. A., J. E. Mickelson, R. B. Thomas, L. C. Patino, B. Cameron, M. J. Carr, M. D. Feigenson, and R. L. Edwards (2007), U-series disequilibria in Guatemalan lavas, crustal contamination, and implications for magma genesis along the Central American subduction zone, *J. Geophys. Res.*, *112*, B06205, doi:10.1029/2006JB004589.
- Wolff, J. A., and J. N. Gardner (1995), Is the Valles Caldera entering a new cycle of activity?, *Geology*, *23*, 411–415, doi:10.1130/0091-7613(1995)023<0411:ITVCEA>2.3.CO;2.
- Zielinski, G. A. (2000), Use of paleo-records in determining variability within the volcanism climate system, *Quat. Sci. Rev.*, *19*, 417–438, doi:10.1016/S0277-3791(99)00073-6.
- Zindler, A., and S. Hart (1986), Chemical geodynamics, *Annu. Rev. Earth Planet. Sci.*, *14*, 493–571.